Black hole spin of Cyg X-1 determined from the softest state ever observed

Takafumi Kawano[1], Chris Done[2,3], Shin'ya Yamada[4], Hiromitsu Takahashi[1], Magnus Axelsson[4], and Yasushi Fukazawa[1]

[1]*Department of Physical Science, Hiroshima University, 1-3-1 Kagamiyama, Higashi-Hiroshima, Hiroshima 739-8526, Japan*

[2]*Centre for Extragalactic Astronomy, Department of Physics, University of Durham, Durham, UK*

[3]*Institute of Space and Astronautical Science (ISAS), Japan Aerospace Exploration Agency (JAXA), Kanagawa, Japan*

[4]*Department of Physics, Tokyo Metropolitan University, Tokyo, Japan*

tkawano@hep01.hepl.hiroshima-u.ac.jp

(Received 2016 October 11; accepted 2017 January 19)

Abstract

We show the softest ever spectrum from Cyg X-1, detected in 2013 with Suzaku. This has the weakest high energy Compton tail ever seen from this object, so should give the cleanest view of the underlying disk spectrum, and hence the best determination of black hole spin from disk continuum fitting. Using the standard model of a disk with simple non-thermal Comptonisation to produce the weak high energy tail gives a high spin black hole. However, we get a significantly better fit by including an additional, low temperature thermal Comptonisation component, which allows a much lower black hole spin. Corroboration of the existence of an additional Compton component comes from the frequency dependent hard lags seen in the rapid variability in archival high/soft state data. These can not be explained if the continuum is a single non-thermal Comptonisation component, but are instead consistent with a radially stratified, multi zone Comptonisation spectrum, where the spectrum is softer further from the black hole. A complex multi-zone Comptonisation continuum is required to explain both spectra and timing together, and this has an impact on the derived black hole spin.

Key words: accretion, accretion disks — X-rays: binaries — X-rays: individuals (Cyg X-1)

1. Introduction

Cyg X-1 was the first black hole candidate to be identified, so is one of the best studied. However, it has some differences compared to the majority of black hole binaries in our Galaxy. It is a persistent rather than transient system, showing that the outer disk is always above the hydrogen ionization instability (van Paradijs 1996). However, even though the system has a high mass companion star, the mass accretion rate from this is probably not high enough for the disk to remain stable in purely Roche lobe overflow, so the disk may be partly wind fed (Coriat et al. 2012).

While the resulting mass accretion rate onto the black hole is rather stable, its value is close to that of dramatic spectral transition, so the system shows strong spectral variability. It switches between the Compton dominated low/hard state towards the disk dominated high/soft state. This is probably the result of a change in the nature of the accretion flow from a hot, optically thin, geometrical thick (advection dominated) accretion flow to a cool, optically thick, geometrically thin disk (see e.g. the review Done et al. 2007). In Cyg X-1 this spectral switch occurs across only a factor 2-3 change in overall luminosity (Zdziarski et al. 2002). This is very different to the transient systems, where the mass accretion rate rises dramatically from quiescence to outburst, and the state transition takes place against a background of a strongly increasing mass accretion rate (e.g. the compilation of Dunn et al. 2010). This may be the origin of the differences seen in the luminosity of the hard-to-soft spectral state change between Cyg X-1 and the transients. The transients show large scale hysteresis, where the hard-to-soft transition during the rapid outburst rise can occur at a much higher (up to at least a factor of 10) luminosity than the reverse transition on the decline, and where the luminosity of the hard-to-soft transition itself is variable between different outbursts of the same source (e.g. Smith et al. 2002; Maccarone & Coppi 2003; Gierliński & Newton 2006; Gladstone et al. 2007; Yu & Yan 2009; Dunn et al. 2010). By contrast, in Cyg X-1, the hysteresis is only small scale, less than a factor of 2-3, and the hard-to-soft transition luminosity is fairly stable (Smith et al. 2002; Zdziarski et al. 2002; Meyer et al. 2007).

The transients often show high/soft spectra which are almost completely dominated by the disk, and where the disk peak temperature and luminosity vary together as expected for a constant inner disk radius as the mass accretion rate changes. This gives confidence that this radius is a fundamental property of the system, as expected if this is the innermost stable circular orbit. This opens a way to measure black hole spin if the system parameters are known accurately (e.g. the reviews by Remillard & McClintock 2006; Done et al. 2007). However, in Cyg X-1 the high/soft state spectra always have a fairly strong tail of emission to high energies (e.g. Negoro et al. 2010), showing that there is a non-negligible fraction of the accretion power which is not dissipated in the thin disk. This could mean that Cyg X-1 never quite makes a full transition, so that the accretion disk never quite reaches down to the last stable circular

orbit, and/or that the coronal emission is fed directly from the stellar wind rather than via the accretion disk (Sugimoto et al. 2016). This latter idea might explain its rather different X-ray variability power spectra compared to high/soft states with similarly strong tails in the transients (Done & Gierliński 2005).

Whatever the origin, the strong tail in the high/soft state of Cyg X-1, it makes the spectra difficult to model as it has complex curvature. Early fits to 0.7-200 keV broadband data from Cyg X-1 required an additional low temperature thermal Comptonisation component as well as the more usual high/soft state components of a disk, high energy Compton tail and its reflection from the disk (Gierliński et al. 1999; Zdziarski et al. 2002). However, while these fits used sophisticated models for the Comptonisation (with both thermal and non-thermal electrons), they used rather simple models of the accretion disk spectra which assumed zero spin. Instead, more recent fits have used some of the best current models for the disk emission in full general relativity, but only included simple Comptonisation models, where the electrons have a single non-thermal power law distribution (Gou et al. 2011; Gou et al. 2014; Tomsick et al. 2014; Walton et al. 2016). These fits require a very high spin black hole, in sharp contrast to the earlier fits with thermal and non-thermal Comptonisation which fit the data with a zero spin black hole disk model. Unlike the transients, Cyg X-1 does not show a wide range in luminosity for its high/soft state, so the apparent disk radius cannot be compared across different mass accretion rates to see if it remains constant as predicted by the high spin solution.

Instead, another way to tell the difference between these two very different physical models is fast time variability. The disk does not vary on timescales of less than a few seconds in the high/soft state (e.g. Churazov et al. 2001), so variability on faster timescales must instead be connected to the Comptonization region(s). This fast variability shows that the light curves at higher energies are correlated with those at lower energies, but with a time lag, and this lag gets shorter for faster variability timescales (Miyamoto & Kitamoto 1989; Nowak et al. 1999; Pottschmidt et al. 2000; Grinberg et al. 2014). Such frequency dependent time lags are commonly seen in the low/hard state, where they are now interpreted as fluctuations propagating down through a Comptonising flow which is radially stratified in both spectrum and variability. Slow fluctuations are stirred up at larger radii, where the spectra are softer. These propagate down to modulate the emission from smaller radii where the spectra are harder, giving rise to a lag of the hard band relative to the soft. Faster fluctuations are stirred up closer to the black hole, so they have less far to propagate in order to reach the hard spectral region, thus giving shorter lags (Lyubarskii 1997; Kotov et al. 2001; Arévalo & Uttley 2006; Rapisarda et al. 2016). The high/soft state in Cyg X-1 has frequency dependent time lags in its fast variability (Pottschmidt et al. 2000), so must have radially stratified Compton continuum spectra rather than a single non-thermal Compton component.

Thus the fast time lags strongly support radial stratification of the Comptonisation spectrum from Cyg X-1 rather than a single Comptonisation region. Here we critically reassess

the spin of the high/soft state in Cyg X-1 by combining the complex Comptonisation continuum models with the best current models of the disk spectrum. Additionally, we apply these to the new data from Suzaku where the high energy Compton tail is the weakest ever observed in Cyg X-1, so should give the best view of the intrinsic disk spectrum. We find that a two zone Comptonisation model gives a better fit to the spectrum than a single zone model, and significantly reduces the derived black hole spin.

2. Observations and Data Reduction

Figure 1 shows the Swift/BAT light curve of Cyg X-1[1], with the times of all the Suzaku (Mitsuda et al. 2007) observations superimposed. There are only five Suzaku observations in a high/soft state (BAT count rate of < 0.05), three of which have been already published (2010, 2011: Yamada et al. 2013; 2012: Tomsick et al. 2014). Here we focus on the remaining two pointed observations of the high/soft state of Cyg X-1, taken on 2013 April 8 (ObsID=407015010, hereafter Obs A), and 2013 May 7 (ObsID=407015020, hereafter Obs B).

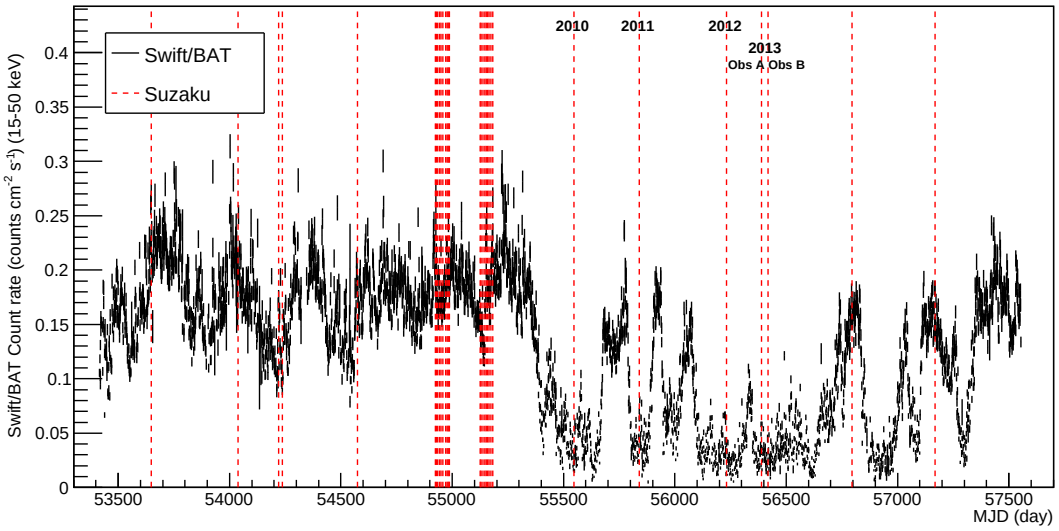

Fig. 1. Light curve of Cyg X-1 observed by Swift/BAT. Red dashed lines show the times of Suzaku observations. There are five Suzaku observations in the high/soft state (defined as BAT count rate $<$ 0.05 counts cm^{-2} s^{-1}).

The XIS0 and XIS1 were operated with 1/4 window mode with 0.3-s burst option, and XIS3 was operated with P-sum (fast timing: Koyama et al. 2007). We conducted the data reduction only for XIS0 as this is the best calibrated. We excluded the core of the CCD image with a radius of 1.4 arcmin in order to reduce the pile-up fraction to below $\sim$3% based on Yamada et al. (2012). To estimate the background level, we analyzed the data during occultation with the GTI selection of $ELV < -5$. The estimated XIS0 background is less than

[1] http://swift.gsfc.nasa.gov/results/transients/CygX-1

0.01% in the lower energy range (∼2.0 keV) and less than ∼1% in the higher energy range (∼10 keV) of the signal events. Hence we ignore this in our analysis.

The HXD-PIN (Takahashi et al. 2007; Kokubun et al. 2007) data reduction is conducted for both observations with the standard procedure, and the ftool of *hxdpinxbpi* was used for tuned background files to create the PIN background spectrum, accounting for both the non-X-ray background (NXB) and the cosmic X-ray background (CXB) (Fukazawa et al. 2009).

The exposure of PIN is 64.51 ks and 20.51 ks for Obs A and Obs B, respectively. Because of the burst option, the corresponding effective exposure of XIS0 is 6.61 ks and 1.39 ks for Obs A and Obs B, respectively. The combination of reduced effective exposure time from excising the piled up core, and the 0.3-s burst option, means that we cannot constrain the fast time lags in the XIS0 data.

Figure 2 shows the 0.5-10 keV XIS0 and 15-30 keV PIN light curves and their hardness ratios for Obs A and Obs B. Plainly there are spectral changes within these two observations. In Obs A there are a few short excursions to very low hardness ratios, but in Obs B this low hardness is sustained over an entire orbit (the fourth segment of Obs B, hereafter Obs B4). Due to the pile up losses, we need at least an orbit of data to accumulate enough signal-to-noise for a good spectrum. Obs B4 has the lowest hardness ratio of any of the orbit segments in Obs A or Obs B.

To investigate the short-term (∼3 ks) variation during Obs B, we extract spectra from each orbit segment. We give details of the time selection in Table 1. Figure 3 left panel shows the time averaged spectra of each of the segments from Obs B, unfolded with a single $\Gamma = 2$ power-law model. It is clear that the 5 - 60 keV flux during Obs B4 is the smallest, as seen in the hardness ratio in Figure 2. Figure 3 right panel shows Obs B4 compared to a compilation of the previous softest spectra seen from Cyg X-1, again unfolded assuming a single $\Gamma = 2$ power-law model. The previous softest spectra seen from Cyg X-1 by Suzaku was from 2010 (Yamada et al. 2013; Gou et al. 2014; Tomsick et al. 2014), which is observed by the XIS0 operated with 1/4 window mode with 0.3-s burst option, where we reduced the data in same way as Obs A and Obs B. Gou et al. (2014) compiled the softest Cyg X-1 spectra where there were both CCD and higher energy data and showed that the Suzaku 2010 data were the softest ever seen at that point. Since Obs B4 is significantly softer, this means it is the softest spectrum yet observed for which there are both CCD data to constrain the disk and higher energy data to constrain the tail.

There are more pointed RXTE observations than CCD datasets. Grinberg et al. (2014) uniformly analyzed all the archival RXTE data, characterizing their spectra with a phenomenological model of a disk plus broken power law with exponential cutoff. We use their model and fit this to Obs B4 over their 3-100 keV energy range. This gives a low energy spectral index of $\Gamma_1 \sim 4.0$, steeper than their steepest index of $\Gamma_1 \sim 3.63$ (Grinberg et al. 2014). Thus Obs B4 is the softest spectrum yet detected from Cyg X-1.

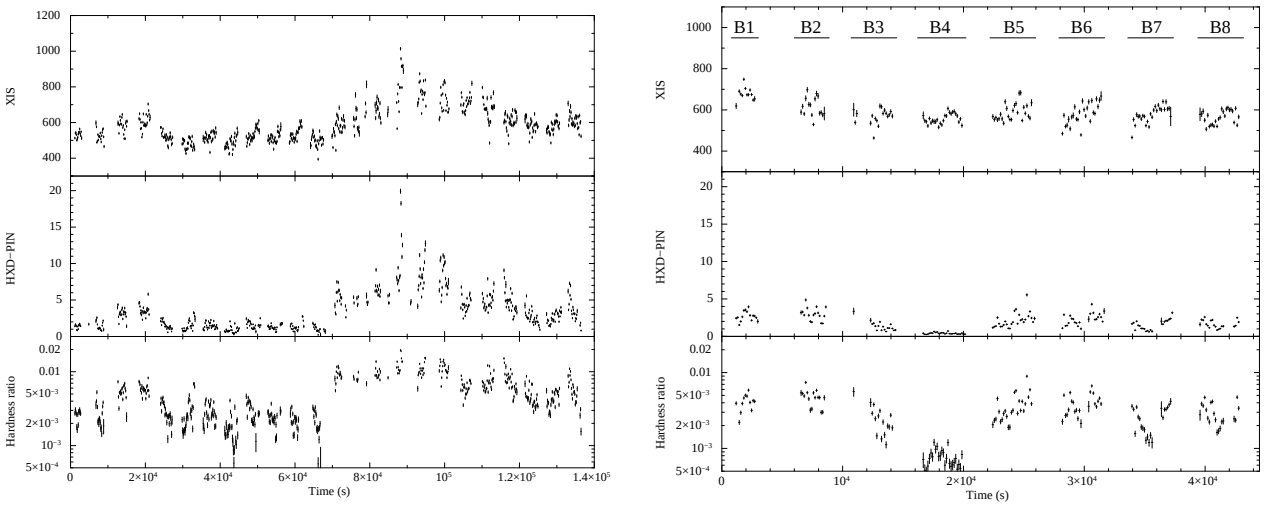

Fig. 2. The light curves with bin of 128 sec observed by Suzaku during Obs A (Left), and that of Obs B (Right). Top: The light curve of the XIS in 0.5 – 10.0 keV. Middle: The light curve of the PIN in 15 –30 keV. Bottom: The hardness ratio between PIN (15 –30 keV) and XIS (0.5 – 10.0 keV). Obs B4 has the lowest 15-30 keV flux and smallest hardness ratio of any orbital segment in Obs A or B.

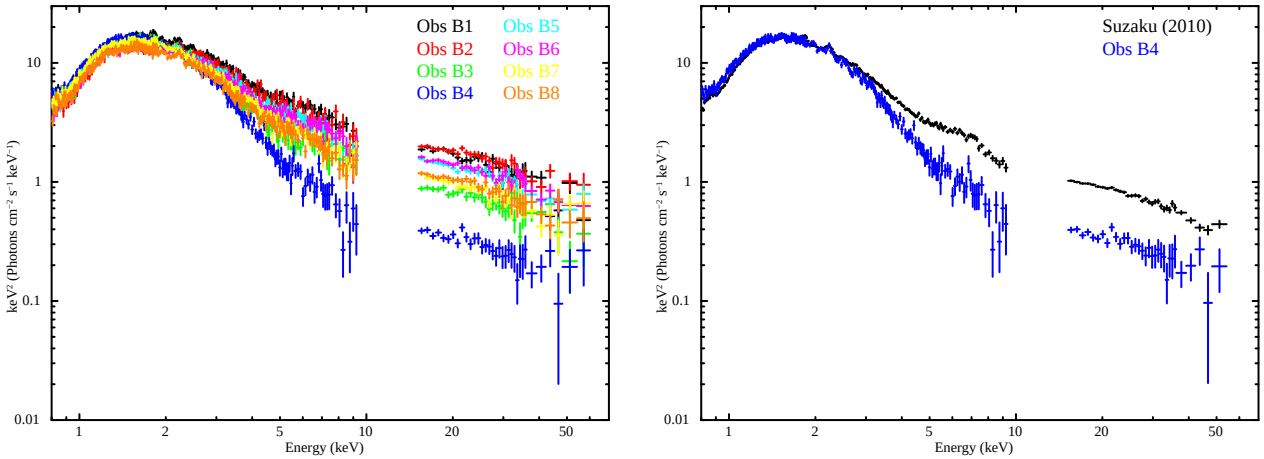

Fig. 3. Left: The XIS, PIN spectrum during Obs B1 (black), Obs B2 (red), Obs B3 (green), and Obs B4 (blue), Obs B5 (light blue), Obs B6 (magenta), Obs B7 (yellow), and Obs B8 (orange), removing the instrumental responses. Right: The comparison between 2010 data (black) of Suzaku (used in Gou et al. 2014) and Obs B4 (blue).

Table 1. The new observations of Cyg X-1 in the high/soft state with Suzaku, together with details of the data extraction of the 2010 data used in Figure 3 right.

Observation	Obs ID	Obs start	Obs end	Exposure [ks] XIS	Exposure [ks] PIN
Obs A	407015010	2013-04-08 02:17:18	2013-04-09 23:00:19	6.61	64.51
Obs B	407015020	2013-05-07 02:13:17	2013-05-07 14:34:19	1.39	20.51
B1		2013-05-07 02:17:33	2013-05-07 02:43:41	0.19	1.81
B2		2013-05-07 03:47:49	2013-05-07 05:04:13	0.11	2.10
B3		2013-05-07 05:04:13	2013-05-07 05:54:45	0.13	2.04
B4		2013-05-07 06:37:01	2013-05-07 07:30:23	0.22	3.45
B5		2013-05-07 08:12:35	2013-05-07 09:05:57	0.19	3.45
B6		2013-05-07 09:48:11	2013-05-07 11:27:33	0.18	2.97
B7		2013-05-07 11:27:33	2013-05-07 12:17:07	0.19	2.38
B8		2013-05-07 12:59:23	2013-05-07 13:52:39	0.19	2.31
2010	905006010	2010-12-17 00:10:26	2010-12-17 18:41:36	2.99	35.50

3. Data Analysis

We use XSPEC version 12.9.0n for all spectral fitting, and give 90% confidence errors on all parameters ($\Delta\chi^2 = 2.706$). We fix the system parameters of distance, black hole mass and disk inclination at $D = 1.86$ kpc, $M = 14.8\ M_\odot$, and $i = 27.1$ deg (Reid et al. 2011; Orosz et al. 2011). The solar abundance table is set to Wilms et al. (2000), and iron abundance is set to 1. We use data from 0.8-8 keV for XIS0, and 15-60 keV for the PIN, but we calculate all models over the range 0.1-1000 keV using the energies extend command as they include convolution components. Additionally, in the following analysis, we fixed the relative normalization CONST of the XIS and PIN at 1.15[2].

3.1. Disk with non-thermal Comptonisation

At first, we follow the model which is used in Gou et al. (2014), where the spectrum is assumed to consist of a relativistic disk (KERRBB: Li et al. 2005), with color temperature correction fixed to 1.7 (Shimura & Takahara 1995), which acts as the source of seed photons for non-thermal Comptonization (SIMPL: Steiner et al. 2009). The SIMPL model in its original form only calculates the sum of the disk and Comptonised photons, whereas only the Comptonised photons are reflected. We thus use the extension of this model, CSIMPL (Kolehmainen et al. 2014) as it allows the Compton tail to be separated from the unscattered disk photons by setting the up scattering switch to 2. We denote this as CSIMPL(2) (Compton scattering component), whereas CSIMPL(1) is the sum of the unscattered disk and Comptonised photons as in SIMPL. Gou et al. (2014) used the XILLVER tables of García et al. (2014) in order to describe the reflection from the disc. These have the most up-to-date treatment of atomic physics, but assume that the illuminating spectrum is a power law, i.e. that source of seed photons for

[2] http://www.astro.isas.jaxa.jp/suzaku/doc/suzakumemo/suzakumemo-2008-06.pdf

Compton scattering is outside of the bandpass. This is not true in our data. Instead we use the XILCONV model which converts the XILLVER reflection table models into a convolution for use with any continuum (Kolehmainen et al. 2011), parameterized by the ionization parameter $\xi = L/(nR^2)$ of the illuminated disc. We then convolved this with the relativistic smearing model RELCONV (Dauser et al. 2014) in order to model reflection from the disc. Gou et al. (2014) used TBABS (Wilms et al. 2000) for the absorption model, however we use TBNEW_GAS, which is an updated version[3]. The full model is then given by:

disk and Comptonization of disk photons (Standard model)

CONST $*$ TBNEW_GAS(CSIMPL(1) $\otimes$ KERRBB + RELCONV $\otimes$ XILCONV(CSIMPL(2) $\otimes$ KERRBB))

We initially tried to determine the best fit parameters of the relativistic reflection from the data, but there are too many free parameters (potentially three for a broken power law emissivity in RELCONV, then another three which are the relative reflection normalization, iron abundance and ionization parameter in XILCONV) for the data quality. We follow Gou et al. (2014) and fix the radial illumination emissivity to a single power law of index of 2.5, fix the abundance to solar, set the reflector solid angle to unity, the inner radius of RELCONV is set to unity, i.e. tied to the spin dependent innermost stable circular orbit, and leaving only $log(\xi)$ as a single free parameter. We note that if we leave additional parameters free, their values cannot be constrained and the fit is not improved.

The fitting results are shown in Figure 4, with parameters given in Table 2. This model gives a high spin, $a_* \sim 0.95$, similar to the results of Gou et al. (2014) even though the scattered fraction is significantly lower than in their data. While the fit is adequate, the PIN residuals in Fig.4 have some discrepancies below 20 keV, showing that the data are not well described by the high energy tail used in this model. A flatter spectral index would give a better fit at these energies, but the steeper index is required in order to fit the lower energy emission. Allowing more parameters to be free does not improve the fit, and as described above the values for the extra parameters cannot be constrained. Instead, the discrepancies likely indicate that the data would be better fit by two different Comptonisation components (Gierliński et al. 1999; Zdziarski et al. 2002). Such a scenario is also more compatible with the observed time lags, and we therefore explore more complex Comptonisation models, where there are two components.

3.2. Complex Comptonisation

We add in an additional thermal Comptonisation component (hereafter called the +thermal model). This is a fairly good approximation (Gierliński & Done 2003) to the combined thermal and non-thermal Comptonisation model used by Gierliński et al. (1999) to fit the ASCA

[3] http://pulsar.sternwarte.uni-erlangen.de/wilms/research/tbabs/

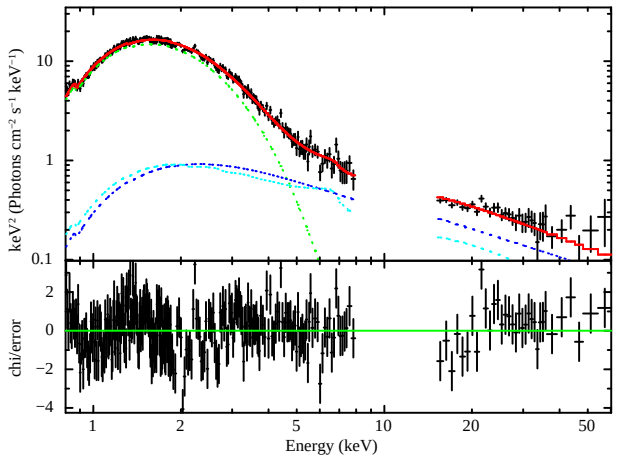

Fig. 4. The fitting results of Obs B4. Assuming Standard disk model (disk and Comptonization of disk photons, corresponding to Gou et al. 2014), red: total, green: KERRBB , blue: Comptonization of KERRBB , cyan: reflection of Comptonization.

and RXTE soft state data from Cyg X-1 (which is only slightly harder than the Suzaku 2010 data). However, their model was a single zone Comptonisation model, where both thermal and non-thermal electrons co-exist in the same region. Instead, our +thermal model explicitly has two separate Comptonisation components, which can be radially separated as required to explain the time lags.

We assume that the low temperature Comptonisation region is itself the seed photons for the non thermal corona (see below), and use COMPTT to describe the continuum shape from Comptonization of soft photons (Titarchuk 1994). We reflect both Comptonisation components, as we are assuming that the thermal electrons can also illuminate the disc. We approximate the disc itself by KERRBB as before.

We note that KERRBB does not fully capture all the physics of our physical picture, where there is a disk which extends down close to (but not necessarily reaches) the last stable circular orbit of the black hole, and where the disk has a standard color temperature correction only down to some radius, below which the color temperature correction is significantly higher, effectively giving rise to the low temperature, additional Comptonised emission. KERRBB instead assumes that the disc extends down to the last stable circular orbit, with fixed color temperature correction. The KERRBB models will then contain more high energy emission than a standard disc which truncates above the last stable circular orbit (leading to an underestimate of black hole spin). However, the gravitational energy released below this truncation should power the low temperature Comptonisation. Including this power in the KERRBB model would increase the inferred disc luminosity, leading to an overestimate of black hole spin. Since these two effects have opposite effects, and since there are no models available which combine inhomogeneous disc structure with fully general relativistic ray tracing (see Kubota & Done 2016 for an inhomogeneous disc structure with approximate relativistic effects), we simply note that

deriving spin is complex and probably not very robust when the spectra are not dominated by a standard disc component.

disk and thermal/non-thermal Comptonization and reflection (+thermal)

CONST $*$ TBNEW_GAS(KERRBB + CSIMPL(1) $\otimes$ COMPTT + RELCONV $\otimes$ XILCONV(CSIMPL(1) $\otimes$ COMPTT))

This gives a significantly better fit to the data, at more than 5σ confidence level by F-test (Protassov et al. 2002), and results in a significantly lower spin which is poorly constrained (See Table 2). The best fit model is shown in Figure 5. The emission which was previously fit as the highest temperature emission from the disk, driving the high spin, is now fit instead as the Comptonization component (but note the caveats above on deriving spin).

For completeness we also fit our data using the full model for thermal and non-thermal electrons used by Gierliński et al. (1999). This allows us to compare to previous results where the complex continuum was fit by a single-zone Comptonization model. We use the EQPAIR[4], model, which has been used for both black hole binaries and AGN (e.g. Zdziarski et al. 1996; Zdziarski et al. 1998). It is a sophisticated physical model which takes into account multiple heating and cooling processes in a single zone region. This derives the self consistent electron distribution from acceleration/heating balanced with cooling from both Coulomb collisions and Comptonisation. Coulomb collisions act to thermalize the low energy electrons, whereas Comptonisation cooling preserves a power law electron distribution. Thus the steady state electron distribution is hybrid, being thermal at low energies but with a power law tail due to Compton cooling dominating at high energies (Poutanen & Coppi 1998; Coppi 1999; Zdziarski et al. 2001; Hjalmarsdotter et al. 2016).

We assume completely non-thermal acceleration, described by a single power law injected electron distribution with index $\Gamma_{\rm inj}$. We allow this index to be free, and fix the lower and upper limits of the electron Lorentz factors to the default values of 1.3 and 1000, respectively. Coulomb cooling depends on the density of electrons in the region which is proportional to the optical depth, $\tau_{\rm p}$, divided by the size scale. We fix the size scale to the default of $R = 10^7$ cm (around $10R_g$, see Gierliński et al. 1999), but have $\tau_{\rm p}$ be a free parameter. Compton cooling depends on the density of seed photons, so is $\propto L_{bb}$ divided by the size scale, which is parameterized via the soft seed photon compactness, $\ell_{bb} \propto L_{bb}/R = 10$ (fixed, see Gierliński et al. 1999). The seed photon distribution in EQPAIR can be either a blackbody, or a simple Schwarzschild black hole model (`diskpn`: Gierliński et al. 1999). We use the `diskpn` option, which has two free parameters, namely the peak disk temperature ($\rm kT_{bb}$) and intrinsic normalization (norm), which is used as the overall normalization of EQPAIR.

The full model is:

non-relativistic disk with fully hybrid electrons and their reflection (eqpair)

[4] http://www.astro.yale.edu/coppi/eqpair/eqpap4.ps

CONST ∗ TBNEW_GAS(EQPAIR + RELCONV ⊗ XILCONV ⊗ EQPAIR)

The EQPAIR model returns both the Comptonisation resulting from the hybrid electron distribution and the unComptonised seed photons. However, our fits have a fairly high optical depth, so only a fraction $\exp(-\tau_{\rm p})$ of these unComptonised seed photons escape. Thus the spectrum is mainly the Comptonisation alone, so we reflect the entire EQPAIR continuum to get a good approximation to the reflection from the Comptonisation components. This gives a slightly worse χ^2 value than the +thermal model above, but is more constrained (has three fewer free parameters) so this is not significant. The inferred intrinsic `diskpn` component has a very similar spectral shape to the KERRBB component in the +thermal model, and the complex EQPAIR Comptonisation is very similar in shape to the sum of the separate thermal and non-thermal Comptonisation components in the +thermal model. However, while this shows that a single zone model can reproduce most of the complex curvature, we again stress that a single-zone model can not explain the time lag behavior (Pottschmidt et al. 2000; Grinberg et al. 2014).

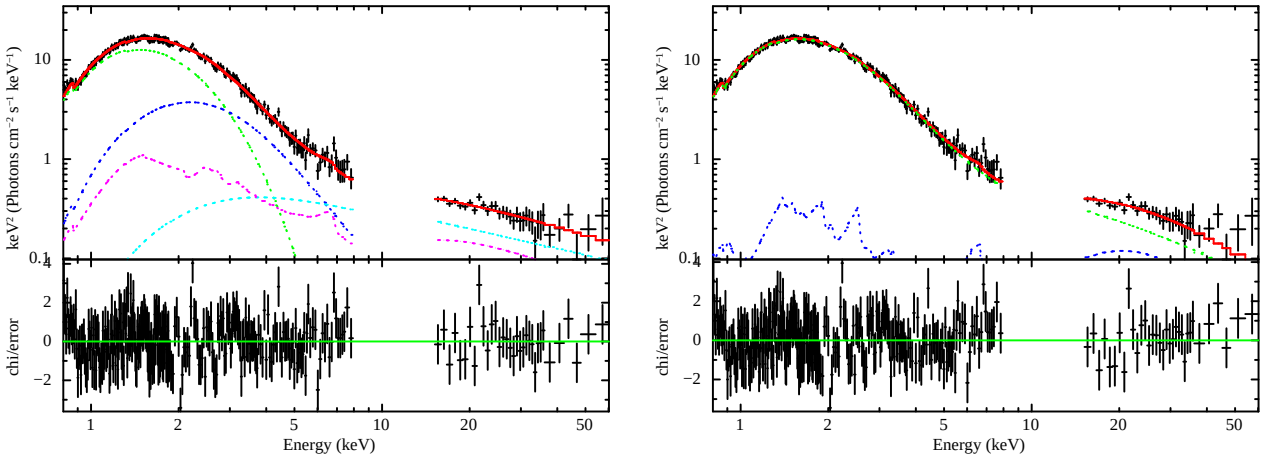

Fig. 5. The fitting results of Obs B4. Left: +thermal (disk and thermal/non-thermal Comptonization and reflection) model, red: total, green: KERRBB , blue: COMPTT , cyan: Comptonization of COMPTT, magenta: reflection of COMPTT and Comptonization Right: eqpair (non-relativistic disk with fully hybrid electrons and their reflection) model, red: total, green: EQPAIR, blue: reflection of EQPAIR.

4. Discussion and Conclusions

The 2013 Suzaku data include the softest ever spectrum seen from Cyg X-1. This means that these data have the smallest contamination from the high energy Compton tail, so should give the best determination of black hole spin from disk continuum fitting. However, we see clear evidence (more than 5σ of F-test) that there is additional low energy Comptonisation. Including this component significantly lowers the derived black hole spin compared to standard models where there is only a disk and high energy Compton tail.

Previous modeling of this low temperature thermal Comptonisation component was

Table 2. Results of fitting the spectrum of B4

Component	Parameter	Standard	+thermal	eqpair
TBNEW_GAS	N_H [10^{22} cm^{-2}]	$0.65^{+0.03}_{-0.02}$	$0.68^{+0.01}_{-0.03}$	$0.69^{+0.02}_{-0.02}$
CSIMPL	Γ	$2.93^{+0.11}_{-0.05}$	$2.67^{+0.18}_{-0.16}$	—
	FracSctr	$0.028^{+0.009}_{-0.003}$	$0.07^{+0.06}_{-0.02}$	—
KERRBB[1]	eta	0 (fixed)	0 (fixed)	—
	a_*	$0.95^{+0.01}_{-0.01}$	$0.80^{+0.08}_{-0.30}$	—
	Mdd [g s^{-1}]	$0.18^{+0.01}_{-0.01}$	$0.24^{+0.06}_{-0.03}$	—
	rflag	1 (fixed)	1 (fixed)	—
	lflag	0 (fixed)	0 (fixed)	—
COMPTT[2]	T_0 [keV]	—	$0.44^{+0.16}_{-0.04}$	—
	kT [keV]	—	$3.52^{+28.73}_{-1.65}$	—
	taup	—	$1.66^{+10.99}_{-0.62}$	—
	norm	—	$1.37^{+1.63}_{-0.87}$	—
XILCONV	log(ξ)	>3.79	$4.00^{+0.27}_{-0.63}$	$4.18^{+0.28}_{-0.47}$
EQPAIR[3]	l_h/l_s	—	—	$0.11^{+0.02}_{-0.01}$
	l_{bb}	—	—	10 (fixed)
	kT_{bb} [keV]	—	—	$0.39^{+0.01}_{-0.02}$
	l_{nt}/l_h	—	—	1 (fixed)
	γ_{min}	—	—	1.3 (fixed)
	γ_{max}	—	—	1000 (fixed)
	Γ_{inj}	—	—	$5.0^{+0.0\dagger}_{-0.3}$
	radius [cm]	—	—	10^7 (fixed)
	τ_p	—	—	$1.51^{+1.48}_{-0.50}$
	norm	—	—	$2.76^{+0.51}_{-0.45}$
	χ^2/d.o.f.	364.57/288	320.63/284	328.88/287

Standard disk model: disk and Comptonization of disk photons

+thermal model: disk and thermal/non-thermal Comptonization and reflection

eqpair model: non-relativistic disk with fully hybrid electrons and their reflection

[1]eta, rflag (a self-irradiation switch flag) and lflag (limb-darkening switch flag) are fixed to the default values.

[2]we fix the geometry switch at the default of 1 (disk).

[3]the internal eqpair reflection is fixed at zero, and all parameters of eqpair associated with this internally generated reflection model are frozen to their default values so that we can use the newer reflection models of XILCONV.

See the text for parameter definitions.

[†]the upper limit of Γ_{inj} is pegged to 5.0.

done using a single zone hybrid (thermal plus non-thermal) Comptonisation, which naturally produces low temperature thermal Comptonised emission even if the electrons are accelerated by purely non-thermal processes. These self consistent models derive the steady state electron distribution by balancing heating/acceleration with Coulomb and Compton cooling (Coppi 1999, Gierliński et al. 1999). However, the fast time lags in these data (Pottschmidt et al. 2000; Grinberg et al. 2014) require that the Comptonisation is radially stratified, rather than arising from a single zone model. Then it seems more plausible that there are really two spatially

separated electron distributions, with the low temperature thermal Comptonisation produced at larger radii, and non-thermal Comptonisation (or more likely, a true hybrid Comptonisation component) produced closer to the black hole (see also Gierliński & Done 2003; Hjalmarsdotter et al. 2016; Kubota & Done 2016).

One possibility for the origin of the low temperature Comptonisation region is that it could be from the disk itself. Cyg X-1 has a long term mass accretion rate which is close to the major hard-to-soft spectral transition, and it is not at all clear whether the source ever fully reaches the classic high/soft state seen in other, brighter, black hole binaries. Other low inclination systems such as GX 339−4 and XTE J1817−330 show ultra soft disk dominated spectra in their lowest luminosity soft states, where the disk dominated spectra have the lowest temperature. In Cyg X-1 the ratio of unabsorbed 6-10 keV/2-6 keV flux in our softest spectrum is 0.05 not < 0.03 as observed in GX 339−4 (Muñoz-Darias et al. 2013). Either Cyg X-1 does not quite reach the soft state proper, or the spin in Cyg X-1 is much higher than that of GX 339−4. We note that reflection fits generally give an extremely high spin for GX 339−4 (e.g. Ludlam et al. 2015 but see Kubota & Done 2016), while continuum fitting allows low spin solutions (Kolehmainen & Done 2010).

In the context of the truncated disk model for the spectral transitions (e.g. Esin et al. 1997; the review by Done et al. 2007), an incomplete transition means that the truncated inner disk is still reforming, condensing out of the hot inner flow (Meyer et al. 2007). Hence its vertical structure could be somewhat different than that of a standard thin disk. In particular, any remaining large scale magnetic fields could give pressure support (see e.g. Sądowski 2016 and references therein), perhaps producing a transition Comptonised region between a fully condensed, outer thin disk and the hot inner flow.

The spectrum we see could then be a consequence of the disk structure in a failed hard-to-soft spectral transition. Other failed hard-to-soft (or very long intermediate state) transitions are reviewed in e.g. Negoro et al. (2010); Negoro et al. (2014). Of these, XTE J1753−0127 also shows a similarly very soft Comptonised spectrum appearing on a failed hard to soft transition at very low luminosity. However, it showed more standard disk spectra during higher luminosity failed hard to soft transitions (Shaw et al. 2016), so it is not at all clear what is the trigger for this different behavior. We also note that similarly complex Comptonisation is also seen in the much higher luminosity system GRS 1915+105, where again its inclusion lowers the derived black hole spin (compare McClintock et al. 2006 with Middleton et al. 2006).

While we cannot do a full spectral-timing analysis on our data due to limitations of the instrument modes, we note that the previous high/soft states with stronger tails used RXTE PCA data (Gou et al. 2011; Gou et al. 2014; Tomsick et al. 2014; Walton et al. 2016). Thus the fast time lags in these spectra can be used to determine the soft Compton component contribution unambiguously. We strongly urge full spectral-timing analyses wherever possible in order to get independent constraints on continuum complexity.

Acknowledgements

We acknowledge earlier work on these Cyg X-1 data by Akifumi Yoshikawa. This work is supported by Japan Society for the Promotion of Science (JSPS). CD acknowledges support from a JSPS Invitation Fellowship for research in Japan (long term) L16518, and STFC funding under grant ST/L00075X. S.Y is supported by Grant-in-Aid for JSPS Kakenhi 15H05438/15H00785. MA is an International Research Fellow of the JSPS. We thank the referee for their comments, which greatly improved the clarity of the paper.

References

Arévalo, P., & Uttley, P. 2006, MNRAS, 367, 801
Churazov, E., Gilfanov, M., & Revnivtsev, M. 2001, MNRAS, 321, 759
Coppi, P. S. 1999, High Energy Processes in Accreting Black Holes, 161, 375
Coriat, M., Fender, R. P., & Dubus, G. 2012, MNRAS, 424, 1991
Dauser, T., García, J., Parker, M. L., Fabian, A. C., & Wilms, J. 2014, MNRAS, 444, L100
Done, C., Gierliński, M., & Kubota, A. 2007, A&A Rev., 15, 1
Done, C., & Gierliński, M. 2005, MNRAS, 364, 208
Dunn, R. J. H., Fender, R. P., Körding, E. G., Belloni, T., & Cabanac, C. 2010, MNRAS, 403, 61
Esin, A. A., McClintock, J. E., & Narayan, R. 1997, ApJ, 489, 865
Fukazawa, Y., Mizuno, T., Watanabe, S., et al. 2009, PASJ, 61, S17
García, J., Dauser, T., Lohfink, A., et al. 2014, ApJ, 782, 76
Gierliński, M., Zdziarski, A. A., Poutanen, J., et al. 1999, MNRAS, 309, 496
Gierliński, M., & Done, C. 2003, MNRAS, 342, 1083
Gierliński, M., & Newton, J. 2006, MNRAS, 370, 837
Gladstone, J., Done, C., & Gierliński, M. 2007, MNRAS, 378, 13
Gou, L., McClintock, J. E., Reid, M. J., et al. 2011, ApJ, 742, 85
Gou, L., McClintock, J. E., Remillard, R. A., et al. 2014, ApJ, 790, 29
Grinberg, V., Pottschmidt, K., Böck, M., et al. 2014, A&A, 565, A1
Hjalmarsdotter, L., Axelsson, M., & Done, C. 2016, MNRAS, 456, 4354
Kokubun, M., Makishima, K., Takahashi, T., et al. 2007, PASJ, 59, 53
Kolehmainen, M., & Done, C. 2010, MNRAS, 406, 2206
Kolehmainen, M., Done, C., & Díaz Trigo, M. 2011, MNRAS, 416, 311
Kolehmainen, M., Done, C., & Díaz Trigo, M. 2014, MNRAS, 437, 316
Kotov, O., Churazov, E., & Gilfanov, M. 2001, MNRAS, 327, 799
Koyama, K., Tsunemi, H., Dotani, T., et al. 2007, PASJ, 59, 23
Kubota, A., & Done, C. 2016, MNRAS, 458, 4238
Li, L.-X., Zimmerman, E. R., Narayan, R., & McClintock, J. E. 2005, ApJS, 157, 335
Ludlam, R. M., Miller, J. M., & Cackett, E. M. 2015, ApJ, 806, 262
Lyubarskii, Y. E. 1997, MNRAS, 292, 679
Maccarone, T. J., & Coppi, P. S. 2003, MNRAS, 338, 189

McClintock, J. E., Shafee, R., Narayan, R., et al. 2006, ApJ, 652, 518
Meyer, F., Liu, B. F., & Meyer-Hofmeister, E. 2007, A&A, 463, 1
Middleton, M., Done, C., Gierliński, M., & Davis, S. W. 2006, MNRAS, 373, 1004
Mitsuda, K., Bautz, M., Inoue, H., et al. 2007, PASJ, 59, 1
Miyamoto, S., & Kitamoto, S. 1989, Nature, 342, 773
Muñoz-Darias, T., Coriat, M., Plant, D. S., et al. 2013, MNRAS, 432, 1330
Negoro, H., & Maxi Team 2010, The First Year of MAXI: Monitoring Variable X-ray Sources, 6
Negoro, H., & MAXI Team 2014, Suzaku-MAXI 2014: Expanding the Frontiers of the X-ray Universe, 128
Nowak, M. A., Vaughan, B. A., Wilms, J., Dove, J. B., & Begelman, M. C. 1999, ApJ, 510, 874
Orosz, J. A., McClintock, J. E., Aufdenberg, J. P., et al. 2011, ApJ, 742, 84
Pottschmidt, K., Wilms, J., Nowak, M. A., et al. 2000, A&A, 357, L17
Poutanen, J., & Coppi, P. S. 1998, Physica Scripta Volume T, 77, 57
Protassov, R., van Dyk, D. A., Connors, A., Kashyap, V. L., & Siemiginowska, A. 2002, ApJ, 571, 545
Rapisarda, S., Ingram, A., Kalamkar, M., & van der Klis, M. 2016, MNRAS, 462, 4078
Reid, M. J., McClintock, J. E., Narayan, R., et al. 2011, ApJ, 742, 83
Remillard, R. A., & McClintock, J. E. 2006, ARA&A, 44, 49
Sądowski, A. 2016, MNRAS, 462, 960
Shaw, A. W., Gandhi, P., Altamirano, D., et al. 2016, MNRAS, 458, 1636
Shimura, T., & Takahara, F. 1995, ApJ, 445, 780
Smith, D. M., Heindl, W. A., & Swank, J. H. 2002, ApJ, 569, 362
Steiner, J. F., Narayan, R., McClintock, J. E., & Ebisawa, K. 2009, PASP, 121, 1279
Sugimoto, J., Mihara, T., Kitamoto, S., et al. 2016, PASJ, 68, S17
Takahashi, T., Abe, K., Endo, M., et al. 2007, PASJ, 59, 35
Titarchuk, L. 1994, ApJ, 434, 570
Tomsick, J. A., Nowak, M. A., Parker, M., et al. 2014, ApJ, 780, 78
van Paradijs, J. 1996, ApJL, 464, L139
Walton, D. J., Tomsick, J. A., Madsen, K. K., et al. 2016, ApJ, 826, 87
Wilms, J., Allen, A., & McCray, R. 2000, ApJ, 542, 914
Yamada, S., Uchiyama, H., Dotani, T., et al. 2012, PASJ, 64, 53
Yamada, S., Negoro, H., Torii, S., et al. 2013, ApJL, 767, L34
Yu, W., & Yan, Z. 2009, ApJ, 701, 1940
Zdziarski, A. A., Johnson, W. N., & Magdziarz, P. 1996, MNRAS, 283, 193
Zdziarski, A. A., Poutanen, J., Mikolajewska, J., et al. 1998, MNRAS, 301, 435
Zdziarski, A. A., Grove, J. E., Poutanen, J., Rao, A. R., & Vadawale, S. V. 2001, ApJL, 554, L45
Zdziarski, A. A., Poutanen, J., Paciesas, W. S., & Wen, L. 2002, ApJ, 578, 357